

# Optical bandedge of diluted magnetic semiconductors: difference between II-VI and III-V-based DMSs

Masao Takahashi\*

Kanagawa Institute of Technology  
1030 Shimo-Ogino, Atsugi-shi, 243-0292, Japan

(Dated: May 1, 2019)

Applying the dynamical coherent potential approximation to a simple model, we have theoretically studied the behavior of the optical bandedge in diluted magnetic semiconductors (DMSs). For  $A_{1-x}^{II}\text{Mn}_x\text{B}^{\text{VI}}$ -type DMS, the present study reveals that the linear relationship between exchange-splitting  $\Delta E_{ex}$  and the averaged magnetization  $|x\langle S_z \rangle|$  widely holds for different values of  $x$ . The ratio,  $\Delta E_{ex}/x\langle S_z \rangle$ , however, depends not only the exchange strength but also the band offset. Furthermore, the present study reveals that in the low dilution of  $\text{Ga}_{1-x}\text{Mn}_x\text{As}$  the optical bandedge exists not at the bandedge of the impurity band but near the bottom of host band. The optical bandedge behaves as if the exchange interaction is ferromagnetic although the antiferromagnetic exchange interaction actually operates at Mn site. We conclude that the spin-dependent shift of the carrier states between the impurity band and host band accompanying with the change of magnetization causes the apparently ferromagnetic behavior of the optical bandedge which was reported in the magnetoreflection measurement of  $\text{Ga}_{1-x}\text{Mn}_x\text{As}$ .

PACS numbers: 75.50.Pp, 71.23.-k, 71.70.Gm

## I. INTRODUCTION

In order to study the effect of the  $sp$ - $d$  exchange interaction between a carrier (an  $s$  conduction electron or  $p$  hole) and localized magnetic moments ( $d$  spins) together with magnetic and chemical disorder in DMSs, we have previously introduced a simple model for  $A_{1-x}\text{Mn}_x\text{B}$ -type DMSs [1]. In this model, the local potentials of nonmagnetic ( $A$ ) ions in a semiconducting compound ( $AB$ ) are substituted randomly, with mole fraction ( $x$ ), by the local potentials that include the exchange interaction between a carrier and the localized spin moment on a Mn (denoted by  $M$ ) ion. Thus, the potential to which a carrier is subjected at a site differs depending on whether the site is occupied by an  $A$  ion or  $M$  ion. The Hamiltonian  $H$  is given by

$$H = \sum_{m,n,\mu} \varepsilon_{mn} a_{m\mu}^\dagger a_{n\mu} + \sum_n u_n, \quad (1.1)$$

where  $u_n$  is either  $u_n^A$  (on the  $A$  site) or  $u_n^M$  (on the  $M$  site) depending on the ion species occupying the  $n$  site:

$$u_n^A = E_A \sum_{\mu} a_{n\mu}^\dagger a_{n\mu}, \quad (1.2)$$

$$u_n^M = E_M \sum_{\mu} a_{n\mu}^\dagger a_{n\mu} - I \sum_{\mu,\nu} a_{n\mu}^\dagger \sigma_{\mu\nu} \cdot \mathbf{S}_n a_{n\nu}. \quad (1.3)$$

Here,  $a_{n\mu}^\dagger$  and  $a_{n\mu}$  are, respectively, the creation and annihilation operators for a carrier with spin  $\mu$  on the  $n$  site. The transfer-matrix element between  $m$  and  $n$ ,

$\varepsilon_{mn}$ , is assumed to be independent of the types of constitutional atoms which occupy the  $m$  and  $n$  sites. In II-VI-based DMSs of the  $A_{1-x}^{II}\text{Mn}_x\text{B}^{\text{VI}}$  type,  $E_A$  ( $E_M$ ) represents a nonmagnetic local potential on the  $A^{2+}$  ( $\text{Mn}^{2+}$ ) sites. In III-V-based DMSs such as  $\text{Ga}_{1-x}\text{Mn}_x\text{As}$ , the spin-independent potential  $E_M$  ( $< 0$ ) can be regarded as a screened Coulomb attractive potential between a carrier (hole) and the  $\text{Mn}^{2+}$  ion (acceptor center). The exchange interaction between the carrier and localized spin  $\mathbf{S}_n$  of the Mn site  $n$  is expressed by  $-I a_{n\mu}^\dagger \sigma_{\mu\nu} \cdot \mathbf{S}_n a_{n\nu}$ , where  $\sigma_{\mu\nu}$  represents the element of the Pauli spin matrices. Throughout this article, we disregard the electron-electron, hole-hole, and/or electron-hole interactions.

The virtual crystal approximation (VCA) is widely employed to describe the extended states in II-VI-based DMSs [2]. The VCA is a first-order perturbation theory with respect to the  $sp$ - $d$  exchange interaction and/or the band offset energy ( $E_M - E_A$ ). In standard VCA, first molecular field approximation (MFA) is applied, replacing  $\mathbf{S}_n$  by the thermal average  $\langle \mathbf{S}_n \rangle$  taken over all Mn site. Second, the local potential  $u_n$  is replaced by configuration averaged one,

$$u_n^{\text{VCA}} = (1-x)u_n^A + x\langle u_n^M \rangle, \quad (1.4)$$

$$= \sum_{\mu} [(1-x)E_A + x(E_M - I\sigma_{\mu\mu}^z \langle S_z \rangle)] a_{n\mu}^\dagger a_{n\mu}, \quad (1.5)$$

for every site, where  $S_z$  is the  $z$ -component of  $\mathbf{S}_n$ . Note  $\langle S_x \rangle = \langle S_y \rangle = 0$  because the magnetization is assumed to be along the  $z$ -axis. A major advantage of the VCA is to employ the periodic Hamiltonian

$$H^{\text{VCA}} = \sum_{m,n,\mu} \varepsilon_{mn} a_{m\mu}^\dagger a_{n\mu} + \sum_n u_n^{\text{VCA}}, \quad (1.6)$$

instead of Eq. (1.1). In the VCA picture, therefore, the carrier "sees" an effective potential  $u^{\text{VCA}} = (1-x)E_A +$

\*Electronic address: taka@gen.kanagawa-it.ac.jp

$x(E_M \mp I\langle S_z \rangle)$  at all site, where  $-(+)$  is for up- (down-) spin of the carrier. No spin-flip process of the carrier is considered. The VCA leads to the exchange energy splitting

$$\Delta E_{ex}^{VCA} = 2xI\langle S_z \rangle. \quad (1.7)$$

Thus, the VCA apparently explains the energy splitting between  $\sigma^+$  and  $\sigma^-$  transition of  $A$  exciton in DMS [2, 3]

$$\Delta E = N_0(\alpha - \beta)x\langle S_z \rangle \quad (1.8)$$

if we assume  $2I$  to be the exchange constant  $N_0\alpha$  for conduction electrons and  $N_0\beta$  for valence electrons, respectively. Furthermore, the VCA explains the linear interpolation expression of the energy gap  $E_g$

$$E_g(x) = E_g(0) + xV_{\text{eff}}, \quad (1.9)$$

where  $V_{\text{eff}} \equiv E_g(1) - E_g(0)$ . Equation (1.9) is experimentally observed for a given composition and temperature in most of II-VI-based DMS when the atoms of the group II element are replaced by Mn [2].

There exist, however, some experimental facts that indicate that the application of the VCA is limited. Among the them, we have already tackled some problems: the anomalous behavior of  $E_g$  (bowing effect) in wide-gap DMSs [1], the enhancement of  $N_0\beta$  with  $x \rightarrow 0$  observed in  $\text{Cd}_{1-x}\text{Mn}_x\text{S}$  [4], and asymmetric splitting of Zeeman energy components [5]. In the previous works, applying the coherent potential approximation (CPA) to the present model, we studied the carrier states of paramagnetic ( $\langle S_z \rangle = 0$ ) and completely ferromagnetic ( $\langle S_z \rangle = S$ ) cases. In the present work, extending the previous approach for the case of a finite  $\langle S_z \rangle$ , we study the nature and property of carrier states in DMSs.

According to the VCA the exchange splitting energy is proportional to  $x\langle S_z \rangle$  and the coefficient is equal to  $N_0(\alpha - \beta)$  (see Eq. (1.8)). In  $\text{Zn}_{1-x}\text{Mn}_x\text{Te}$  [6] and  $\text{Cd}_{1-x}\text{Mn}_x\text{Te}$  [7], however, it is reported that the spin splitting energy is proportional to  $x\langle S_z \rangle$  but the coefficient decreases with the increase in  $x$ . This may be explained by taking the higher order effect of the exchange interaction into account, although imperfect treatment based on the second order perturbation was already done [8].

Another strong motivation of the present work is the elucidation of the sign and amplitude of the  $p$ - $d$  exchange interaction in  $\text{Ga}_{1-x}\text{Mn}_x\text{As}$ . In the early stage of research, the *ferromagnetic* (FM) coupling ( $N_0\beta > 0$ ) was reported on the basis of the polarized magnetoreflection measurement [9]. However, the exchange interaction between  $p$  holes and  $d$  spins is experimentally proved later to be *antiferromagnetic* (AFM) [10, 11, 12]. On the mechanism of the so-called carrier-induced ferromagnetism in  $\text{Ga}_{1-x}\text{Mn}_x\text{As}$ , which has attracted much attention in recent years [13], we have already proposed a theory based on the present model [14]. According to the theory, the occurrence of ferromagnetism closely relates with the magnetic impurity band which is formed due

to the incorporation of Mn to GaAs. When an impurity band exists, the optically observed bandedge may be different from the bandedge of the impurity band. Thus, it is highly desirable to clarify what the optical measurement has detected. Throughout the present work, we investigate the difference in the optical bandedge between II-VI-based and III-V-based DMSs.

This paper is organized as follows. In Sec. II we briefly formulated the dynamical CPA on the bases of the multiple-scattering theory. The results and discussion for the behavior of the optically observed bandedge and the carrier states in II-VI-based DMS (or the case with no magnetic impurity level) is given in Sec. III. Section IV is devoted for  $\text{Ga}_{1-x}\text{Mn}_x\text{As}$ . Section V contains the conclusion.

## II. DYNAMICAL COHERENT POTENTIAL APPROACH (CPA)

### A. Dynamical CPA condition

We shall confine our discussion to the so-called one-particle picture. Hereafter we assume the carrier is  $p$  hole, although the result does not depend on the character of the carrier. A carrier moving in a DMS is subjected to disordered potentials which arise not only from substitutional disorder but also from thermal fluctuation of  $d$  spins through the  $p$ - $d$  exchange interaction. Furthermore, when magnetization arises, the effective potential for the carrier differs according to the orientation of the carrier spin. In the dynamical CPA [15], the disordered potential is considered in terms of the spin-dependent effective medium where a carrier is subject to a coherent potential,  $\Sigma_{\uparrow}$  or  $\Sigma_{\downarrow}$ , according to the orientation of its spin. The coherent potential  $\Sigma_{\uparrow}$  ( $\Sigma_{\downarrow}$ ) is an energy ( $\omega$ )-dependent complex potential. Then, a carrier moving in this effective medium is described by the unperturbed Hamiltonian  $K$ :

$$K = \sum_{k\mu} (\varepsilon_k + \Sigma_{\mu}) a_{k\mu}^{\dagger} a_{k\mu}. \quad (2.1)$$

Thus, the perturbation term  $V (= H - K)$  is written as a sum over each lattice site:

$$V = \sum_n v_n, \quad (2.2)$$

where  $v_n$  is either  $v_n^A$  or  $v_n^M$ , depending on the ion species occupying the  $n$  site:

$$\begin{aligned} v_n^A &= \sum_{\mu} (E_A - \Sigma_{\mu}) a_{n\mu}^{\dagger} a_{n\mu}, \\ v_n^M &= \sum_{\mu} (E_M - \Sigma_{\mu}) a_{n\mu}^{\dagger} a_{n\mu} - I \sum_{\mu,\nu} a_{n\mu}^{\dagger} \boldsymbol{\sigma}_{\mu\nu} \cdot \mathbf{S}_n a_{n\nu}. \end{aligned} \quad (2.3)$$

$$(2.4)$$

Next, using the reference Green's function  $P$  given by

$$P(\omega) = \frac{1}{\omega - K}, \quad (2.5)$$

we define the matrix  $t^A$  which represents the multiple scattering of carriers due to the  $A$  ion potential embedded in the effective medium by

$$t_n^A = v_n^A [1 - P v_n^A]^{-1}, \quad (2.6)$$

and the matrix  $t^M$  which represents the multiple scattering of carriers due to the  $M$  ion potential embedded in the effective medium by

$$t_n^M = v_n^M [1 - P v_n^M]^{-1}. \quad (2.7)$$

Note that  $K$ , and thus  $P$ , includes no localized spin operator, and that  $t_n^A$  ( $t_n^M$ ) represents the complete scattering associated with the isolated potential  $v_n^A$  ( $v_n^M$ ) in the effective medium. According to the multiple-scattering theory [16, 17], the total scattering operator  $T$ , which is related to  $G \equiv 1/(\omega - H)$  as

$$G = P + PTP, \quad (2.8)$$

is expressed as the multiple-scattering series,

$$T = \sum_n t_n + \sum_n t_n P \sum_{m (\neq n)} t_m + \sum_n t_n P \sum_{m (\neq n)} t_m P \sum_{l (\neq m)} t_l + \dots \quad (2.9)$$

Within the single-site approximation, the condition

$$\langle t_n \rangle_{\text{av}} = 0 \quad \text{for any site } n \quad (2.10)$$

leads to  $\langle T \rangle_{\text{av}} \cong 0$  and thus  $\langle G \rangle_{\text{av}} \cong P$ . Here, we express the average of  $t_n$  over the disorder in the system as  $\langle t_n \rangle_{\text{av}}$ . Since the present system includes both substitutional disorder and the thermal fluctuation of the localized spin on a  $M$  site, the average of the  $t$  matrix is written as

$$\langle t_n \rangle_{\text{av}} = (1 - x)t_n^A + x\langle t_n^M \rangle. \quad (2.11)$$

Here,  $(1 - x)$  and  $x$  are the mole fractions of  $A$  and  $M$  atoms, respectively;  $\langle t^M \rangle$  means the thermal average of  $t^M$  over fluctuating localized spin. In the dynamical CPA, the coherent potential  $\Sigma_\mu$  is decided such that the effective scattering of a carrier at the chosen site embedded in the effective medium is zero on average. Note that the thermal average of off-diagonal  $t$ -matrix elements  $\langle t_{\uparrow\downarrow}^M \rangle = \langle t_{\downarrow\uparrow}^M \rangle = 0$  because the magnetization is assumed to be along the  $z$ -axis. Therefore, the dynamical CPA condition is given by

$$(1 - x)t_{\uparrow\uparrow}^A + x\langle t_{\uparrow\uparrow}^M \rangle = 0, \quad (2.12a)$$

$$(1 - x)t_{\downarrow\downarrow}^A + x\langle t_{\downarrow\downarrow}^M \rangle = 0. \quad (2.12b)$$

For simplicity, the  $t$  matrix elements in the site representation  $\langle n\mu | t | n\nu \rangle$  ( $n$  is a site index,  $\mu, \nu = \uparrow$  or  $\downarrow$ ) are written as  $t_{\mu\nu}$ . The explicit expressions for  $t_{\mu\nu}^A$  and  $t_{\mu\nu}^M$  are given in Appendix A. It is worth noting that in the expression of  $t_{\uparrow\uparrow}^M$  ( $t_{\downarrow\downarrow}^M$ ), the spin-flip processes are properly taken into account. As a result, a single  $t$ -matrix element  $t_{\mu\mu}^M$  depends on both  $\Sigma_\uparrow$  and  $\Sigma_\downarrow$ . Therefore, we solve Eqs. (2.12a) and (2.12b) simultaneously. Note that the diagonal matrix element  $t_{\mu\mu}^M$  involves an operator  $S_z$  which takes the quantum values of  $2S + 1$ ;  $S_z = -S, -S + 1, \dots, S$ . Thus, the thermal average over the fluctuating localized spin is taken as

$$\langle t_{\mu\mu}^M \rangle = \sum_{S_z = -S}^S t_{\mu\mu}^M(S_z) \exp\left(\frac{hS_z}{k_B T}\right) / \sum_{S_z = -S}^S \exp\left(\frac{hS_z}{k_B T}\right), \quad (2.13)$$

where  $h$  denotes the effective field felt by the localized spins. Since there is a one-to-one correspondence between  $\langle S_z \rangle$  and the parameter  $\lambda \equiv h/k_B T$ , we can describe the carrier states in terms of  $\langle S_z \rangle$  instead of  $\lambda$ . In this work, we treat the localized spins classically for simplicity; the actual calculations were performed for  $S = 400$ .

## B. DOS and local DOS

Throughout this work, we assume the model density of states of the semicircular form with a half-bandwidth  $\Delta$ ,

$$\rho(\varepsilon) = \frac{2}{\pi\Delta} \sqrt{1 - \left(\frac{\varepsilon}{\Delta}\right)^2}, \quad (2.14)$$

as an undisturbed density of states. Then, the density of states with  $\mu$  spin,  $D_\mu(\omega)$ , is calculated by

$$D_\mu(\omega) = -\frac{1}{\pi} \text{Im} \int_{-\Delta}^{\Delta} d\varepsilon \frac{\rho(\varepsilon)}{\omega - \varepsilon - \Sigma_\mu(\omega)}. \quad (2.15)$$

for the  $\Sigma_\mu$  determined by the CPA. In all of the present numerical results, we have numerically verified

$$\int_{-\infty}^{\infty} D_\uparrow(\omega) d\omega = \int_{-\infty}^{\infty} D_\downarrow(\omega) d\omega = 1. \quad (2.16)$$

The species-resolved DOS shall help us to understand the nature of the carrier states. We calculate the  $A$ - and  $M$ -site components of the DOS,  $(1 - x)D_\mu^A(\omega)$  and  $x D_\mu^M(\omega)$  ( $\mu = \uparrow$  or  $\downarrow$ ), where  $D_\mu^A(\omega)$  [ $D_\mu^M(\omega)$ ] represents the local DOS associated with the  $A$  ( $M$ ) site (see Appendix B). Note that

$$D_\mu(\omega) = (1 - x)D_\mu^A(\omega) + x D_\mu^M(\omega). \quad (2.17)$$

Since  $D^A(\omega)$  and  $D^M(\omega)$  are normalized, the total number of  $A$ -site states and that of  $M$ -site states are  $1 - x$  and  $x$ , respectively.

### C. Optical absorption spectrum

$A_{1-x}^{\text{II}}\text{Mn}_x\text{B}^{\text{VI}}$ -type DMSs are direct-gap semiconductors, with the band extrema occurring at the  $\Gamma$  point [2]. Upon calculating the optical absorption spectrum, we assume that the transition dipole moments of the  $A$  and  $M$  ions are same. Under this assumption, the optical absorption spectrum is given by the  $k = 0$  components of the DOS. Since the explicit  $k$  dependence of  $\varepsilon_k$  is not employed in the present framework, we assume that  $k = 0$  corresponds to the minimum point of the model band. Therefore, taking  $\varepsilon_0 = -\Delta$ , we define the optical absorption spectrum by: [18]

$$A_\mu(\omega) = -\frac{1}{\pi} \text{Im} \frac{1}{\omega + \Delta - \Sigma_\mu(\omega)}. \quad (2.18)$$

GaAs is a direct-gap semiconductor, whose band extrema exist at the  $\Gamma$  point [19, 20]. In  $\text{Ga}_{1-x}\text{Mn}_x\text{As}$ , the bottom of the conduction band is still at  $\Gamma$  point [21], even though an impurity band forms above the top of the valence band. Therefore, we apply the optical absorption spectrum defined by Eq. (2.18). (see later discussion in Sec. VI).

### D. Optical carrier spin polarization $\mathcal{P}(\omega)$ and spin-coupling strength $Q(\omega)$

In order to investigate the manner of coupling between the carrier spin and the localized spin in DMS, we define the optical carrier spin polarization,  $\mathcal{P}(\omega)$ , by

$$\mathcal{P}(\omega) = \frac{D_\downarrow(\omega) - D_\uparrow(\omega)}{D_\downarrow(\omega) + D_\uparrow(\omega)}. \quad (2.19)$$

with  $E_B = E_M - IS$  ( $E_B = E_M + IS$ ) for a carrier with  $\uparrow$  ( $\downarrow$ ) spin. On the other hand, when  $\langle S_z \rangle = 0$ , we obtain

$$\begin{aligned} \Sigma_b^3 - \Sigma_b^2(2E_M + \Delta) + \Sigma_b \left\{ \left( E_M - IS + \frac{\Delta}{2} \right) \left( E_M + IS + \frac{\Delta}{2} \right) + \frac{\Delta}{2} E_M x \right\} \\ - \frac{\Delta}{2} x \left\{ (E_M - IS)(E_M + IS) + \frac{\Delta}{2} E_M \right\} = 0. \end{aligned} \quad (3.2)$$

As long as an impurity level (band) does not appears, the energy shift of the bandedges calculated by using

Further, we calculate the spin-coupling strength  $Q(\omega)$  defined by (see Appendix B)

$$Q(\omega) \equiv - \frac{\langle \delta(\omega - H) \sigma \cdot \mathbf{S} \rangle / S}{\langle \delta(\omega - H) \rangle} \Big|_{\text{at } M\text{-site}}. \quad (2.20)$$

Note that  $Q(\omega)$  corresponds to  $-\langle \cos \theta \rangle$ , where  $\theta$  is the *angle* between the carrier spin and localized spin at the  $M$  site. Therefore,  $Q(\omega)$  represents the strength of the spin coupling at  $M$ -site.

## III. RESULTS AND DISCUSSION FOR II-VI-BASED DMS

### A. Approximate expression for the bandedge energy shift

Here we briefly summarize the approximate treatment to consider the behavior of the bandedge energy, although we can numerically solve the equation for the bandedge energy shift. Hereafter, we set  $E_A \equiv 0$  as the origin of the energy. For the energy of the bottom of the band,  $\omega_b$ , we assume that  $\omega_b = -\Delta + \Sigma(\omega_b)$  in the dynamical CPA condition Eq. (2.12). Then, when  $\langle S_z \rangle = S$ , we obtain the approximate expression for the bandedge energy shift  $\Sigma_b [= \Sigma(\omega_b)]$ : [4]

$$\frac{\Sigma_b}{\Delta} = \frac{1}{2} \left\{ \left( \frac{1}{2} + \frac{E_B}{\Delta} \right) - \sqrt{\left( \frac{1}{2} + \frac{E_B}{\Delta} \right)^2 - 2x \left( \frac{E_B}{\Delta} \right)} \right\}, \quad (3.1)$$

the cubic equation for  $\Sigma_b$ : [5]

Eqs. (3.1) and (3.2) give good approximate values, as

shown in the present work. Hence, on the basis of the approximate expression we investigate the relationship between the exchange integral  $N_0\beta$  obtained by optically measurement and the parameters  $E_M$  and  $IS/\Delta$  used in the present model. We define  $N_0\beta$  by using the exchange energy splitting at  $\langle S_z \rangle = S$ , as:

$$N_0\beta = \frac{\Sigma_b(+)-\Sigma_b(-)}{xS}, \quad (3.3)$$

where  $\Sigma_b(+)$  and  $\Sigma_b(-)$  are the solutions of Eq. (3.1) for  $E_B = E_M + IS$  and  $E_B = E_M - IS$ , respectively. Therefore  $N_0\beta$  is a function of  $x$ , and has following limiting values:

$$N_0\beta \rightarrow \frac{2I}{(1+2\frac{E_M}{\Delta})^2 - (2\frac{IS}{\Delta})^2} \quad \text{when } x \rightarrow 0, \quad (3.4a)$$

$$N_0\beta = 2I \quad \text{when } x = 1 \quad (3.4b)$$

### B. Results for $IS/\Delta = -0.4$ and $E_M/\Delta = 0$

To our knowledge, no impurity (acceptor) level has experimentally observed in  $A_{1-x}^{II}\text{Mn}_x\text{B}^{\text{VI}}$ -type DMSs. This implies that the fitting parameters in the present model should be taken as  $|IS + E_M| < 0.5\Delta$  for II-VI-based DMSs. In Figs. 1 ~ 3, we show the results for  $IS = -0.4\Delta$  and  $E_M = 0.0$  as a sampling case of II-VI-based DMSs. We should note here that these parameters may be fit to describe a DMS like  $\text{Cd}_{1-x}\text{Mn}_x\text{S}$  which has the rather strong exchange interaction among II-VI-based DMSs (see Ref. 1).

Figure 1(a) shows how the carrier band is spin-polarized with the development of magnetization. Note that even when  $\langle S_z \rangle = 0$ , the band is not same as the model band. Owing to the disorder of random distribution of  $M$  ion and fluctuation of localized spins, the band has already broaden and the bottom of the band has shifted to lower side from  $\omega_b = -\Delta$ . With increase in  $\langle S_z \rangle$ , the bottom of down-spin band shifts to lower-energy side while accompanying the energy shift of bottom of the up-spin band. The both bandedges agree with each other except the case of  $\langle S_z \rangle = S$ , although the down-spin band is strongly suppressed in the band tail. This is because the spin-flip of up-spin carrier occurs at the energies wherein  $D_{\downarrow}(\omega)$  takes a finite value. In magnetoabsorption and/or magnetorefectivity spectra, on the contrary, the spin splitting band is observed. Thus, the present result for the bandedge shift is very different from the behavior expected from magneto-optical measurements. In Fig. 1 (b), we show the optical absorption spectrum  $A(\omega)$ , that is related to the dipole transition at  $\Gamma$  point. A peak is found in the up- and down-optical absorption spectrum, respectively. Hence, we regard the energy,  $\omega_p(\text{up})$

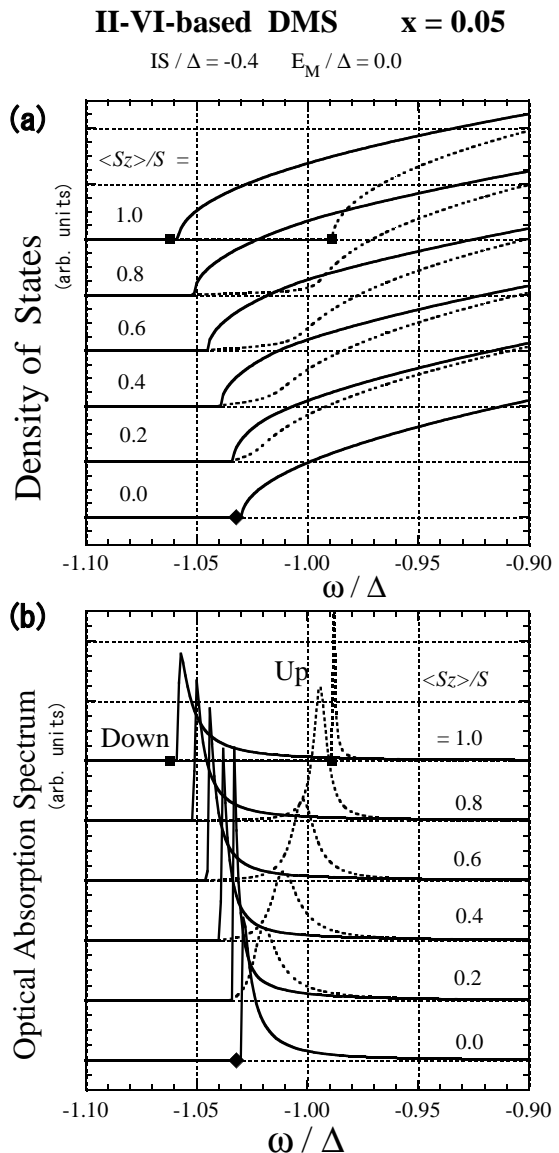


FIG. 1: Results with  $x = 0.05$  as a function of  $\omega/\Delta$  for various values of magnetization: (a) density of states  $D(\omega)$  (b) optical absorption band  $A(\omega)$  in arbitrary unit (arb.units). Solid line is for down-spin carrier, and dotted line is for up-spin carrier. The approximate values of the bandedge energy,  $\omega_b/\Delta$ , calculated using Eqs. (3.1) and (3.2), are dotted on the line of  $\langle S_z \rangle = S$  and  $\langle S_z \rangle = 0$ , respectively. Note that the energy of the bottom of the model band is  $\omega = -\Delta$ .

$[\omega_p(\text{down})]$ , at which the up (down)- spectrum takes a peak, as the up (down)- bandedge energy experimentally observed in optical measurement. In Fig. 2, we display the optical bandedge energies,  $\omega_p(\text{up})$  and  $\omega_p(\text{down})$ , as a function of the  $\langle S_z \rangle$ . The result shows that  $\omega_p(\text{up})$  and  $\omega_p(\text{down})$  are roughly linear in  $\langle S_z \rangle$ . The behavior of the optical bandedge energy reproduces well an asymmetrical splitting of Zeeman energy component; when magnetiza-

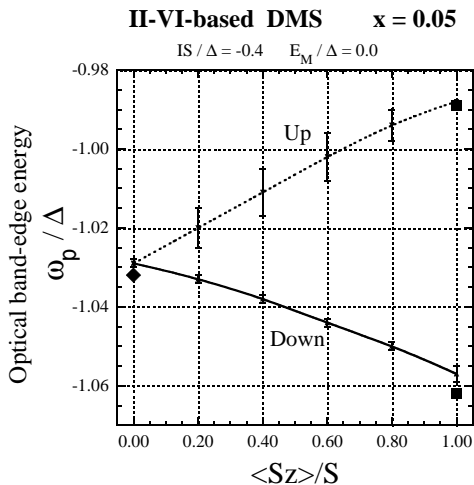


FIG. 2: Optical band-edge energies  $\omega_p/\Delta$  as a function of  $\langle S_z \rangle/S$ . Solid line is for down-spin carrier, and dotted line is for up-spin carrier. Error bar represents a half-peak width. The approximate values of  $\omega_b/\Delta$ , calculated by Eqs. (3.1) and (3.2), are dotted on the line of  $\langle S_z \rangle = S$  and  $\langle S_z \rangle = 0$ , respectively.

tion arises the energy-shift pattern  $\sigma^+$  and  $\sigma^-$  transition term of the A exciton is asymmetric relative to the position of  $\langle S_z \rangle = 0$ . The asymmetric splitting of Zeeman energy component has observed not only  $\text{Cd}_{1-x}\text{Mn}_x\text{S}$  [22] but also in  $\text{Cd}_{1-x}\text{Co}_x\text{Te}$  [23]. The half-peak width indicated by error bars in Fig. 2 shows that the peak of the optical spectrum with up-spin is broader than that of down-spin, which may explain the reason why the  $\sigma^-$  peak is broader than  $\sigma^+$  peak in the magnetoabsorption spectra [24, 25].

The VCA presents the picture that a carrier in a DMS moves freely in an uniform medium of effective potential  $u^{VCA} = \mp xI\langle S_z \rangle$ ; the depends on the orientation of the carrier spin. The present study reveals the feature of the carrier in II-VI-based DMS as below. A carrier does not stay with the same probability on each site, but tends to reside longer at Mn site due to the exchange interaction; Although  $x = 0.05$  is assumed, the ratio of the Mn-site component of the DOS to the total DOS  $R(\omega) = 0.2 \sim 0.3$  at the band tail, as shown in Fig. ??(c). The carrier state at A-site shows similar  $\langle S_z \rangle$  dependence to that at Mn site (compare Figs. ??(a) and (b)). The result of  $Q(\omega) \approx 1$  (see Fig. ??(b)) exhibits the strong antiparallel spin coupling (AP-coupling) between carrier's spin and the localized spin realizes at Mn site, and the high values of the optical spin polarization  $\mathcal{P}(\omega)$  (see Fig. ??(a)) suggests that the carrier itinerates over the crystal while holding the effect of the strong AP-coupling. The strong spin-coupling, however, realizes only in the very narrow energy range of bandedge. The results for  $\mathcal{P}(\omega)$  and  $Q(\omega)$ , shown in Fig. ??, suggest that  $Q(\omega) = -\omega/\Delta$  and  $\mathcal{P}(\omega) \approx 0$  in the wide range of

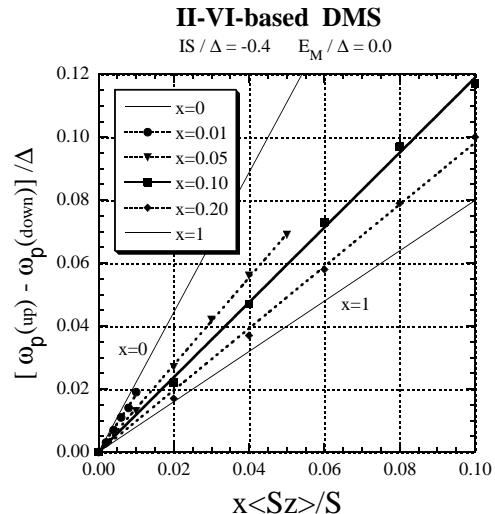


FIG. 3: Exchange splitting  $[\omega_p(\text{up}) - \omega_p(\text{down})]/\Delta$  as a function of  $x\langle S_z \rangle/S$  for various values of  $x$ . The straight lines are adjusted to the best fit the each  $x$  data. The straight lines of  $x = 0$  and  $x = 1$  exhibit the limiting cases given by Eqs. (3.4a) and (3.4b).

energy  $\omega$  as  $(-\Delta \lesssim \omega \lesssim \Delta)$ . This is consistent with the change in  $R(\omega)$ . As the energy  $\omega$  increases beyond  $-\Delta$ , the probability of the carrier to reside Mn-site decreases so that the value of  $\mathcal{P}(\omega)$  rapidly approaches 0.

In Fig. 3, the exchange-splitting energy,  $\omega_p(\text{up}) - \omega_p(\text{down}) = -\Delta E_{ex}$ , is plotted as a function of  $x\langle S_z \rangle$ . The data for each  $x$  are well fitted by a straight line. The slope corresponds to  $|N_0\beta|$  (or  $-\Delta E_{ex}/x\langle S_z \rangle = -N_0\beta$ ). With the increase in  $x$ , the slope of the line decreases. It is worth noting that the straight line with  $x = 1$  agrees with that of VCA. Thus, the present result suggests that the drastic decrease in  $|\Delta E_{ex}|/x\langle S_z \rangle$  slope when  $x$  increases.

Here, we compare the present result with that previously obtained by the second order perturbation. Considering the second-order scattering process due to the exchange interaction, Bhattacharjee [8] showed that not only the coefficient proportional to  $x\langle S_z \rangle$  but also the coefficient proportional to  $x(x\langle S_z \rangle)^{\frac{1}{2}}$  is included in the term of  $(\frac{IS}{\Delta})^2$ . The latter coefficient comes from that the first order correction is taken in to account in the intermediate process of the second-order scattering. According to his result, thus, the exchange splitting energy is not proportional to  $x\langle S_z \rangle$ . On the other hand, the present result suggests the proportional relationship between  $\Delta E_{ex}$  and  $x\langle S_z \rangle$  holds in the wide range of the parameters  $IS$ ,  $E_M$  and  $x$ . The experimental observation in  $\text{Zn}_{1-x}\text{Mn}_x\text{Te}$  [6] and  $\text{Cd}_{1-x}\text{Mn}_x\text{Te}$  [7] shows that the spin-splitting  $\Delta E$  as a function of  $x\langle S_z \rangle$  is a straight line and that the slope  $N_0(\alpha - \beta)$  exhibits a large decrease for high  $x$  values, which seems to support the present result.

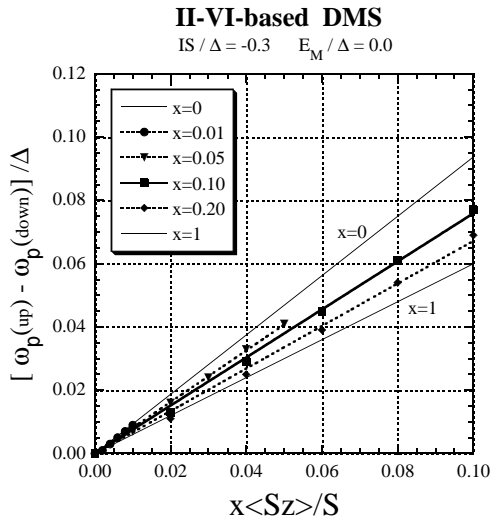


FIG. 4: Same as Fig.3 but for  $IS/\Delta = -0.3$  and  $E_M/\Delta = 0.0$ .

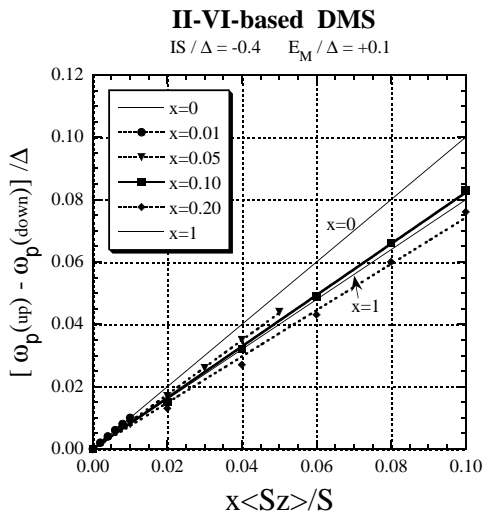


FIG. 5: Same as Fig.3 but for  $IS/\Delta = -0.4$  and  $E_M/\Delta = +0.1$ .

### C. Some other results for II-VI-based DMSs

Figures 4 and 5 are the same results as Fig. 3 but for  $IS = -0.3\Delta$  and  $E_M = 0.0$ , and for  $IS = -0.4\Delta$  and  $E_M = +0.1\Delta$ , respectively. Figures indicate that the linear relationship between exchange splitting and  $x\langle S_z \rangle$  is kept for each case. Furthermore, the results show that not only the reduction in  $|IS|$  but also positive  $E_M$  suppress the effect of multiple scattering. This can be understood as follows. The repulsive interaction due to  $E_M$  prevents the carrier to stay on Mn site longer. Thus, positive  $E_M$  substantially make the effect of the exchange

interaction weaken. On the other hand, negative  $E_M$  assists the carrier to reside on Mn site, resulting in apparently large  $|N_0\beta|$ . Therefore, the present results request us reexamine the VCA and the hypothesis of  $N_0\beta = 2I$  which have been widely accepted for II-VI-based DMSs. We need precise information on the exchange energy, the bandwidth and the band offset energy for more quantitative comparison between theory and experimental observation.

## IV. RESULTS AND DISCUSSION FOR (GA,MN)AS

### A. Model parameters for $\text{Ga}_{1-x}\text{Mn}_x\text{As}$

In this section, we discuss in detail the reason why a positive  $N_0\beta$  is experimentally observed by magneto-optical measurement of (Ga,Mn)As. For  $\text{Ga}_{1-x}\text{Mn}_x\text{As}$ , we take  $\Delta = 2$  eV [26, 27],  $IS = -0.4\Delta$  and  $E_M = -0.3\Delta$ , as the same as previous work [14]. These parameters lead to an impurity level at the energy of  $E_a = -1.057\Delta$  in the dilute limit ( $x \rightarrow 0$ ), which is consistent with an acceptor energy of 0.113eV ( $= 0.057\Delta$ ) [28]. With the increase in  $x$  an impurity band forms around the acceptor level. The impurity band merges into the host valence band at  $x \gtrsim 0.035$  when  $\langle S_z \rangle = 0$ , while the down-spin DOSs unite at  $x \gtrsim 0.017$  when  $\langle S_z \rangle = S$ . The result roughly agrees with the experimental observation of impurity-band-like states [29, 30]. Also this may be related to the insulator-metal transition reported to occur at  $x \sim 0.03$  [31, 32].

### B. Case of low dilution

As the typical case that  $x$  is so small that an impurity band forms separating from the host band irrespective of  $\langle S_z \rangle = S$ , we investigate the case with  $x = 0.005$ ; the results are shown in 6 ~ ?? . As is shown in Fig. 6(a), the magnetic impurity band forms around the impurity level and imitates the model band. The numerical result for the optical absorption spectrum  $A(\omega)$  is shown in Fig. 6(b). We notice that the peak of optical absorption spectrum is almost near the bottom of the *host* band, although the impurity band exists in lower energy region. This can be explained as follows. The states of the impurity band are composed from the states of the wide range values in  $k$  space. The  $k = 0$  component in the impurity band states is nominal. Since the  $A(\omega)$  is related to  $k = 0$  state, the optical absorption spectrum takes negligible values in the impurity band.

As the consequence, the optical band edge,  $\omega_p$ , exists almost at the bottom of the *host* band. Here, we should stress that the energy of the peak in  $A(\omega)$  of up-spin carrier is lower than that of down-spin carrier (or  $\omega_p(\text{up}) < \omega_p(\text{down})$ ), although we have assumed the AFM exchange interaction ( $IS < 0$ ). This implies that

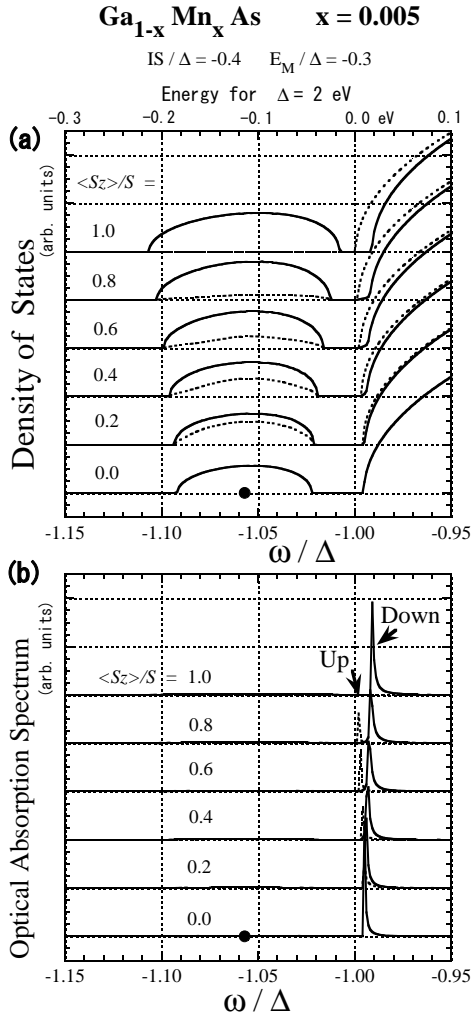


FIG. 6: Results with  $x = 0.005$  as a function of  $\omega/\Delta$  for various values of magnetization: (a) density of states  $D(\omega)$  (b) optical absorption band  $A(\omega)$  in arbitrary unit (arb.units). Solid line is for down-spin carrier, and dotted line is for up-spin carrier. Note that the energy of the bottom of the model band is  $\omega = -\Delta$ . Above the upper horizontal axis of (a), energies for  $\Delta = 2$  eV are graduated in eV;  $\omega = -\Delta$  is taken 0 eV as the origin of the energies. The impurity level  $E_a = -1.057\Delta$  (or  $-0.057\Delta = -0.113$  eV) is indicated by a dot on the line of  $\langle S_z \rangle = 0$ .

the direction of the shift of the optical bandedge is opposite from that predicted by the VCA. This may explain the reason why the FM exchange interaction was reported on the basis of the polarized magnetoreflexion measurement [9], although the exchange interaction between  $p$  holes and  $d$  spins is AFM [10, 11, 12].

In order to verify our picture, we first investigate the manner of coupling between the carrier spin and localized spins. We show the results for  $\mathcal{P}(\omega)$  and  $Q(\omega)$  in Fig.???. The result that  $\mathcal{P}(\omega) \approx \frac{\langle S_z \rangle}{S}$  and  $Q(\omega) \approx 1$  in the impurity band indicates that the strong antiparal-

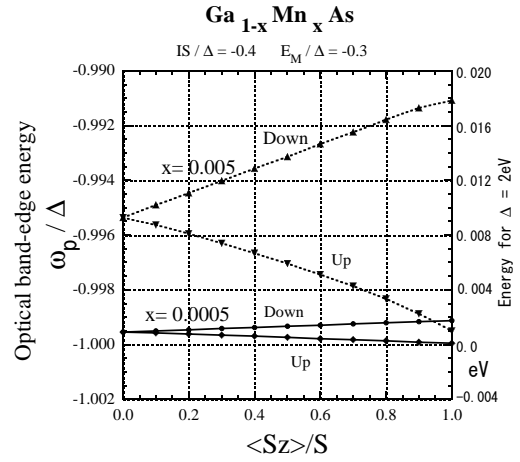


FIG. 7: Optical band-edge energies  $\omega_p/\Delta$  with up- and down-spin as a function of  $\langle S_z \rangle/S$  for  $x = 0.0005$  (solid line) and  $x = 0.005$  (dotted line). Beside the right vertical axis, energies for  $\Delta = 2$  eV are graduated in eV;  $\omega = -\Delta$  is taken 0 eV as the origin of the energies.

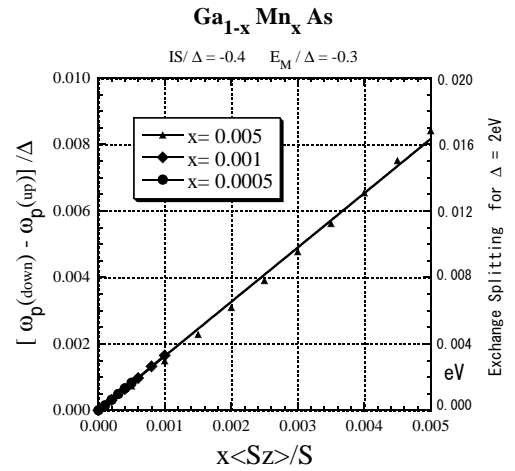


FIG. 8: Exchange splitting  $[\omega_p(\text{down}) - \omega_p(\text{up})]/\Delta$  as a function of  $x\langle S_z \rangle/S$  for  $x = 0.0005, 0.001$ , and  $0.005$ . Beside the right vertical axis, energies for  $\Delta = 2$  eV are graduated in eV. The straight line corresponds to  $[\omega_p(\text{down}) - \omega_p(\text{up})]/x\langle S_z \rangle = 1.31$  eV.

lel spin coupling (AP-coupling) between carrier spin and localized spins occurs therein. Near the bottom of the *host* band, however, we find that  $\mathcal{P}(\omega) \approx -\frac{\langle S_z \rangle}{S}$ , suggesting the parallel spin coupling (P-coupling) therein. On the other hand,  $Q(\omega)$  takes high values suggesting the weak AP-coupling near the bottom of the *host* band. Only when as  $\langle S_z \rangle \gtrsim 0.95S$ ,  $Q(\omega)$  takes negative values near the bottom of the *host* band. Here we should notice the difference in  $\mathcal{P}(\omega)$  and  $Q(\omega)$ . The optical carrier polarization,  $\mathcal{P}(\omega)$ , describes the spin coupling between the carrier's spin and localized spins averaged *all over*



the sites, while  $Q(\omega)$  represents the strength of the spin-coupling at  $M$ -sites. Hence, the result suggests that the bottom of the *host* band apparently behaves as if the carrier spin *ferromagnetically* couples to the localized spins although it may *antiferromagnetically* couples to the localized spins at  $M$ -sites.

Next, we investigate how different way carrier states with up- and down-spin shift as the magnetization develops. The total number of states in the impurity band is  $x$ , irrespective of  $\langle S_z \rangle$ . When  $\langle S_z \rangle = 0$ , the carrier states with up- and down-spin are completely the same, and the numbers of up- and down-spin states in the impurity band are  $x/2$ , respectively. With increase in  $\langle S_z \rangle$ , as shown in Fig. 6(a), the density of states with up-spin in the impurity band is suppressed, and finally vanishes when  $\langle S_z \rangle = S$ . On the other hand, the number of states with down-spin in the impurity band increases from  $x/2$  to  $x$ . The total number of states keeps being 1.0 per a site for each spin (up and down) [see Eq. (2.16)]. With the increase in  $\langle S_z \rangle$ , therefore, the carrier states with up-spin shift from the host band to the impurity band, whereas the carrier states with down-spin shift from the impurity band to the host band.

To examine the mechanism in more detail, we show the result for local DOS in Fig. ???. Figure ??(c) indicates that rather large rate of the impurity band is composed from  $M$ -site states [ $R(\omega) \approx 0.5$ ], in spite of small  $x$  ( $x = 0.005$ ). The total number of impurity states, 0.005, is composed from  $M$ -site component of 0.00246 and  $A$ -site component of 0.00254, irrespective of  $\langle S_z \rangle$ . The result shown in Fig. ??(a) indicates that the shift of the  $A$ -site states occur between the impurity band and *near the bottom of the host band*. Figure ??(b), on the other hand, indicates that the shift of the  $M$ -site states occur between the impurity band and *over the wide energy range of the host band*. This can be explained as follows. The effective local potential for carriers at  $M$ -site is  $E_M + IS = -0.7\Delta$  for AP-coupling while  $E_M - IS = +0.1\Delta$  for P-coupling. The AP-coupling states constitute the magnetic impurity band, whereas the P-coupling states extend over wide range of *host* band due to the positive effective local potential. Thus, the up-spin carrier states at  $M$ -site are the AP-coupling sates in the impurity band when  $\langle S_z \rangle = 0$ , whereas the P-coupling states *spreading over the wide-range energy of host band* when  $\langle S_z \rangle = S$ . The carrier states with down-spin shift in the opposite way. Hence, nominal change occurs *near the bottom of host band* in  $M$ -site component DOS, as shown in ??(b). The present result reveals that the shift in the bottom of the host band is mainly ascribed to that in  $A$ -site component DOS. The spin dependent shift of the  $A$ -site states near the bottom of *host* band results in the shift of optical bandedge. The direction of the shift is opposite from that predicted by the VCA.

In Fig. 7, we show the present result for the optical bandedge energies  $\omega_p$  with up- and down-spins as a function of  $\langle S_z \rangle / S$  for  $x = 0.0005$  and  $0.005$ . The result suggests that the linear relationship between  $\omega_p$  and  $\langle S_z \rangle / S$

well holds in such dilute case that the impurity band forms separate from the host band. In Fig. 8, we plot the exchange splitting  $\omega_p(\text{down}) - \omega_p(\text{up}) [= +\Delta E_{ex}]$  as a function of  $x\langle S_z \rangle / S$  for  $x = 0.0005, 0.001$ , and  $x = 0.005$ . The data are well fitted by a straight line. The  $N_0\beta$  with  $S = 5/2$  deduced from the slop of the straight line is  $+1.31$  eV. Szczytko *et. al* measured the exciton splitting in  $\text{Ga}_{1-x}\text{Mn}_x\text{As}$  with  $x = 0.00047, 0.00027$  and  $0.00022$  by polarized magnetoreflection, and showed that the data are proportional to magnetization, to obtain  $N_0\beta = +2.5 \pm 0.8$  eV [9]. The agreement between the present result and experimentally obtained one is satisfactory. Therefore, we conclude that the spin-dependent shift of the carrier states between the impurity band and host band accompanying with the change of magnetization causes the apparently FM behavior of the optical bandedge.

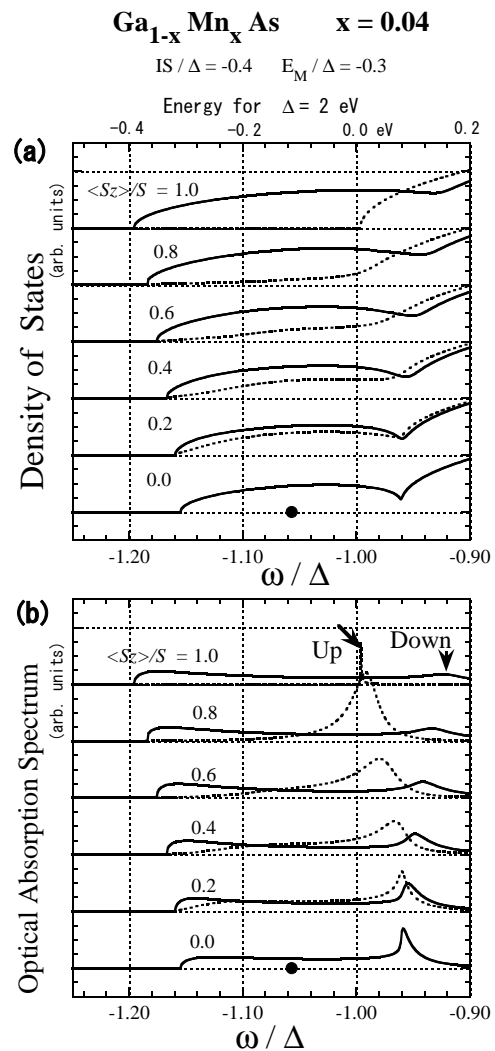


FIG. 9: Same as Fig. 6, but for  $x = 0.04$

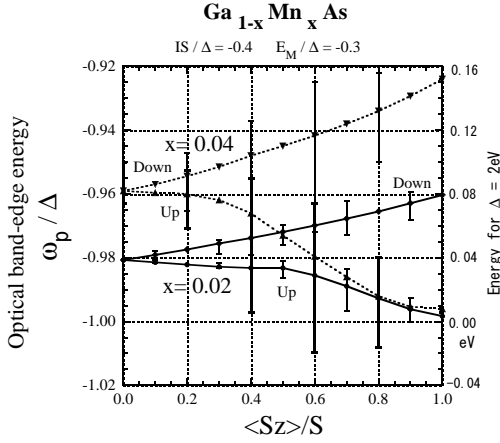


FIG. 10: Optical band-edge energies  $\omega_p/\Delta$  with up- and down-spin as a function of  $\langle S_z \rangle/S$  for  $x = 0.02$  (solid line) and  $x = 0.04$  (dotted line). Error bar represents the half-peak width. Beside the right vertical axis, energies for  $\Delta = 2$  eV are graduated in eV;  $\omega = -\Delta$  is taken 0 eV as the origin of the energies.

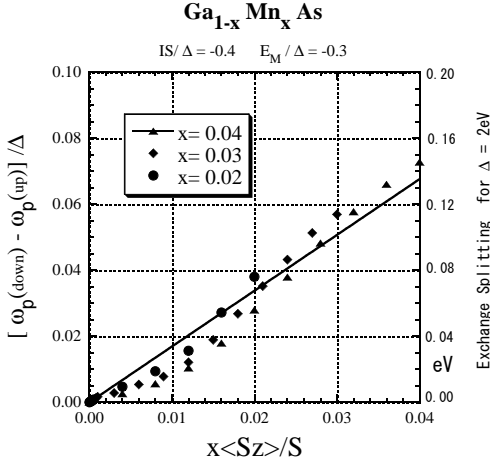


FIG. 11: Exchange splitting  $[\omega_p(\text{down}) - \omega_p(\text{up})]/\Delta$  as a function of  $x\langle S_z \rangle/S$  for  $x = 0.02, 0.03$ , and  $x = 0.04$ . Beside the right vertical axis, energies for  $\Delta = 2$  eV are graduated in eV. The straight line corresponds to  $[\omega_p(\text{down}) - \omega_p(\text{up})]/x\langle S_z \rangle = 1.36$  eV.

### C. Case of moderate dilution

As the typical case that  $x$  is so large that the impurity band merges to the host band irrespective of  $\langle S_z \rangle$ , we investigate the case with  $x = 0.04$ ; the results are shown in Fig.9 ~ ???. In contrast to the case of  $x = 0.005$ , the impurity band and host band have already united to form the band tail, as shown in Fig.9(a). The peak of the optical absorption spectrum is broaden due to the increase of the disorder which is caused by the additional corporation of  $M$  ion, as shown in Fig.9(b). However, the

peak of optical absorption spectrum is not in the bandtail originated from the impurity band but still exists in the energy range near the bottom of the original *host* band. Thus, the direction of the shift in the optical band edge is opposite to that predicted by the VCA, as is the case of  $x = 0.005$ . The results for  $\mathcal{P}(\omega)$  and  $Q(\omega)$ , shown in Fig.??, indicate that the strong AP-coupling realizes in the bandtail, whereas  $\mathcal{P}(\omega)$  shows the weak P-coupling at the energies near the optical bandedge. The result for the shift of the states accompanying the change in  $\langle S_z \rangle$ , deduced from Fig ??, has similar tendency with that of  $x = 0.0005$ , although the merge of the impurity band makes the feature less clear.

In Fig.10, we show the optical band-edge energies,  $\omega_p(\text{up})$  and  $\omega_p(\text{down})$ , as a function of  $\langle S_z \rangle/S$  for  $x = 0.02$  and  $x = 0.04$ . When  $x = 0.04$ , the absorption spectrum of up-spin is broadened. The exchange splitting  $\Delta E_{ex}$  increases monotonically with the increase in  $\langle S_z \rangle/S$ , while the linear relationship hardly holds. In Fig. 11 we plot the exchange splitting,  $\omega_p(\text{down}) - \omega_p(\text{up}) [= +\Delta E_{ex}]$ , as a function of  $x\langle S_z \rangle/S$  for  $x = 0.02, 0.03$ , and  $0.04$ . The data do not fit a straight line well. Note that for  $0.017 \lesssim x \lesssim 0.035$ , the impurity band separating from host band when  $\langle S_z \rangle = 0$  unites to the host band when  $\langle S_z \rangle = S$ . The  $N_0\beta$  deduced from the slope of the straight line in Fig. 11 is  $+1.36$  eV, which is consistent with the experimental observation (see below).

Here we compare the present result with that of magnetoabsorption [12]. Note that the band-gap energy of GaAs is 1.52 eV [11]. In the absorption spectrum (see Fig. 1 in Ref. 12), a rather weak structure is visible below 1.5 eV. We regard the structure as the optical transition related to the *impurity* band, although Szczytko *et al.* disregarded it as the below-the-gap transition. When  $x$  is so large that the impurity band unites the host band, the optical absorption spectrum  $A(\omega)$  takes appreciable values at the energies in the impurity band, as shown in 9(b). In the energy range above 1.5 eV, on the contrary, the absorption band increases monotonously with the increase in the photon energy, which we assign to the optical absorption related with the *host* band. Under the external magnetic field, the edge splits about 0.1 eV, which is the feature of *sp-d* exchange effect but opposite way than for  $\text{Cd}_{1-x}\text{Mn}_x\text{Te}$ . Evaluating the spin splitting as the relative edge shift at high energies as 1.7 eV, they obtained  $N_0(\alpha - \beta) = -2.1$  eV for  $x = 0.032$  and  $-1.7$  eV for  $x = 0.042$ . Thus, they measured the energy shift at the *host* band to obtain the  $N_0(\alpha - \beta)$ . The result is consistent with our view that the optical bandedge near the bottom of original host band behaves as if the exchange interaction is FM although the AFM exchange interaction acutely operates between the carrier and localized spins at Mn site. The values of  $N_0(\alpha - \beta)$  are comparable with  $N_0(\alpha - \beta) = -(2.3 \pm 0.6)$  eV obtained in the very dilute cases of  $x = 0.00022 \sim 0.00047$  [9]. Szczytko *et al.* concluded that the coincident of values of  $N_0(\alpha - \beta)$  for different  $x$  is accidental because they believed the splitting inversion is so caused by the Moss-

Burstein effect that the splitting depends on the carrier concentration. The coincidence, however, might not be accidental because the spin splitting near the bottom of the *host* band was measured in both cases. The states near the bottom of the (original) host band are always almost empty, although the carriers may enter into the impurity band or the bandtail originating from the impurity band. Since the optical transition is related to the states near the bottom of the (original) host band, as shown in this study, the carrier concentration would not significantly affect the exchange splitting optically observed in III-V DMSs. The impurity band and/or bandtail structure changes with the Mn concentration  $x$ . In the absorption band of  $\text{Ga}_{1-x}\text{Mn}_x\text{As}$  experimentally obtained, the impurity-like structure of  $x = 0.042$  more overlaps with the host-band-like structure than that of  $x = 0.032$ . This may be another supporter of our picture.

## V. CONCLUDING REMARKS

In this study, applying the dynamical CPA to a simple model, we investigated the behavior of the optical band-edge in DMSs in a systematic way. For  $A_{1-x}^{\text{II}}\text{Mn}_x\text{B}^{\text{VI}}$ -type DMS, the present study reveals that the linear relationship between exchange-splitting  $\Delta E_{ex}$  and the averaged magnetization  $|x\langle S_z \rangle|$  widely holds for different values of  $x$ . The ratio,  $\Delta E_{ex}/x\langle S_z \rangle$ , however, depends not only the exchange energy ( $IS$ ) but also the band offset ( $E_M$ ). The present theory can qualitatively explain the  $x$  dependency of  $N_0(\alpha - \beta)$  reported in  $\text{Zn}_{1-x}\text{Mn}_x\text{Te}$  [6] and  $\text{Cd}_{1-x}\text{Mn}_x\text{Te}$  [7]. For the quantitative description, however, we need more precise knowledge on the exchange energy, the bandwidth, and the band offset energy. This will be discussed in detail elsewhere. Here, we have to indicate that the present model does not take into account of many features such as multiband effects, band anisotropy, and excitonic structure, which exist in real DMS's. In the CPA, furthermore, the collective mode, correlation and/or clustering effect of localized spins, which may become significant for large  $x$  region, are completely out of scope. These issues remain for future study.

Regarding the  $p$ - $d$  exchange interaction of  $\text{Ga}_{1-x}\text{Mn}_x\text{As}$ , there have been long controversial discussions not only on the amplitude but also even on the sign. The uncertainty has made the model for the carrier-induced ferromagnetism difficult to establish. In the present paper, we have proposed a new interpretation for the experimental result in magneto-optical measurements. A  $\text{Mn}^{2+}$  ion in  $\text{GaAs}$  acts as both an acceptor and a magnetic impurity. Therefore, on the Mn-site, a carrier ( $p$  hole) is subject to the local potential which includes the  $p$ - $d$  exchange interaction together with the attractive Coulomb potential. In the dilution limit, thus, there appears an acceptor level. With the increase in  $x$ , an impurity band forms around the impurity level. In such low dilution that

the impurity band forms separate from host band, the optical band-edge exists not at the band-edge of the impurity band but near the band-edge of host band, as shown in this study. The optical band-edge behaves as if the exchange interaction is ferromagnetic although the antiferromagnetic exchange interaction actually operates at Mn site. We concluded that the spin-dependent shift of the carrier states between the impurity band and host band causes the apparently ferromagnetic shift of the optical band-edge. The conclusion is valid even when  $x$  is so large that the impurity band unites the host band because the optical band-edge exists near the bottom of the original mother band. The present result is consistent with the theory for the mechanism of the carrier-induced ferromagnetism in III-V based DMS's that we have previously proposed [14].

## Acknowledgments

The author is grateful to Professor K. Kubo for his helpful discussion and comments on the present study. This work was supported in part by Grants-in-Aid for Scientific Research Nos. 14540311 from the Ministry of Education, Culture, Sports, Science and Technology of Japan.

## APPENDIX A: DYNAMICAL CPA — $t$ MATRIX FORMALISM

### 1. $t$ matrix elements of $A$ ion embedded in the effective medium

Here we omit the site suffix. The  $t$  matrix elements, which represent the multiple scattering of carriers with  $\uparrow$  ( $\downarrow$ )-spin due to the  $A$  ion potential  $E_A$  embedded in the effective medium  $\Sigma_{\uparrow}$  ( $\Sigma_{\downarrow}$ ), is given by [16]

$$t_{\uparrow\uparrow}^A = \frac{E_A - \Sigma_{\uparrow}}{1 - (E_A - \Sigma_{\uparrow})F_{\uparrow}}, \quad (\text{A1a})$$

$$t_{\downarrow\downarrow}^A = \frac{E_A - \Sigma_{\downarrow}}{1 - (E_A - \Sigma_{\downarrow})F_{\downarrow}}. \quad (\text{A1b})$$

Here,  $F_{\mu}[\equiv F_{\mu}(\omega)]$  is the diagonal matrix element of a propagator  $P$  with respect to the effective medium,  $\Sigma_{\mu}[\equiv \Sigma_{\mu}(\omega)]$  ( $\mu = \uparrow$  or  $\downarrow$ ), and is calculated by

$$F_{\mu} = \langle \mu | P | \mu \rangle = \int_{-\Delta}^{\Delta} d\varepsilon \frac{\rho(\varepsilon)}{\omega - \varepsilon - \Sigma_{\mu}(\omega)}, \quad (\text{A2})$$

where  $\rho(\omega)$  is the model DOS. For  $\rho(\omega)$  given by Eq. (2.14), we obtain

$$F_{\mu}(\omega)\Delta = 2 \left\{ \left( \frac{\omega - \Sigma_{\mu}}{\Delta} \right) - \sqrt{\left( \frac{\omega - \Sigma_{\mu}}{\Delta} \right)^2 - 1} \right\} \quad (\text{A3})$$

Note that  $t_{\uparrow\downarrow}^A = t_{\downarrow\uparrow}^A = 0$ .

## 2. $t$ matrix elements of $M$ ion embedded in the effective medium

In accordance with the definition of the  $t$  matrix, Eq. (2.7), we have

$$t^M[1 - Pv^M] = v^M. \quad (\text{A4})$$

Equation (A4) is written in the spin-matrix element expression as

$$t_{\uparrow\uparrow}^M - t_{\uparrow\uparrow}^M F_{\uparrow} v_{\uparrow\uparrow}^M - t_{\uparrow\downarrow}^M F_{\downarrow} v_{\uparrow\downarrow}^M = v_{\uparrow\uparrow}^M, \quad (\text{A5})$$

$$t_{\downarrow\downarrow}^M - t_{\downarrow\downarrow}^M F_{\downarrow} v_{\downarrow\downarrow}^M - t_{\downarrow\uparrow}^M F_{\uparrow} v_{\downarrow\uparrow}^M = v_{\downarrow\downarrow}^M. \quad (\text{A6})$$

---


$$t_{\uparrow\uparrow}^M[(1 - F_{\uparrow} v_{\uparrow\uparrow}^M)(F_{\downarrow} v_{\uparrow\downarrow}^M)^{-1} - F_{\uparrow} v_{\uparrow\downarrow}^M(1 - F_{\downarrow} v_{\downarrow\downarrow}^M)^{-1}] = v_{\uparrow\uparrow}^M(F_{\downarrow} v_{\uparrow\downarrow}^M)^{-1} + v_{\uparrow\downarrow}^M(1 - F_{\downarrow} v_{\downarrow\downarrow}^M)^{-1}. \quad (\text{A7})$$


---

By using the following definitions and/or symbols introduced for simplicity,

$$V_{\uparrow} \equiv v_{\uparrow\uparrow}^M = E_M - IS_z - \Sigma_{\uparrow}, \quad (\text{A8a})$$

$$V_{\downarrow} \equiv v_{\downarrow\downarrow}^M = E_M + IS_z - \Sigma_{\downarrow}, \quad (\text{A8b})$$

$$v_{\uparrow\downarrow}^M = -IS_- \quad (\text{A8c})$$

$$v_{\downarrow\uparrow}^M = -IS_+ \quad (\text{A8d})$$

$$U_{\uparrow} \equiv E_M - I(S_z - 1) - \Sigma_{\uparrow}, \quad (\text{A8e})$$

$$U_{\downarrow} \equiv E_M + I(S_z + 1) - \Sigma_{\downarrow}, \quad (\text{A8f})$$

$$W_{\uparrow} \equiv I^2 S_- S_+ = I^2[S(S+1) - S_z^2 - S_z], \quad (\text{A8g})$$

$$W_{\downarrow} \equiv I^2 S_+ S_- = I^2[S(S+1) - S_z^2 + S_z], \quad (\text{A8h})$$

and recalling the commutation relationships between the components of  $\mathbf{S}$ ,

$$S_- S_z = (S_z + 1)S_-, \quad (\text{A9})$$

$$(S_+)^{-1} = [S(S+1) - (S_z)^2 - S_z]^{-1}(S_-), \quad (\text{A10})$$

we obtain an explicit expression for  $t_{\uparrow\uparrow}^M$  using no more approximations. Other  $t$ -matrix elements are obtained

Then, Eq. (A5)  $\times (F_{\downarrow} v_{\uparrow\downarrow}^M)^{-1}$  + Eq. (A6)  $\times (1 - F_{\downarrow} v_{\downarrow\downarrow}^M)^{-1}$  leads to an equation including  $t_{\uparrow\uparrow}$  only ( $t_{\uparrow\downarrow}$  is canceled):

by a similar procedure. The resulting expressions are

$$t_{\uparrow\uparrow}^M = \frac{V_{\uparrow} + F_{\downarrow}(W_{\uparrow} - V_{\uparrow}U_{\downarrow})}{1 - F_{\downarrow}U_{\downarrow} - F_{\uparrow}[V_{\uparrow} + F_{\downarrow}(W_{\uparrow} - V_{\uparrow}U_{\downarrow})]}, \quad (\text{A11a})$$

$$t_{\downarrow\downarrow}^M = \frac{V_{\downarrow} + F_{\uparrow}(W_{\downarrow} - V_{\downarrow}U_{\uparrow})}{1 - F_{\uparrow}U_{\uparrow} - F_{\downarrow}[V_{\downarrow} + F_{\uparrow}(W_{\downarrow} - V_{\downarrow}U_{\uparrow})]}, \quad (\text{A11b})$$

$$\begin{aligned} t_{\uparrow\downarrow}^M &= \frac{1}{1 - F_{\downarrow}U_{\downarrow} - F_{\uparrow}[V_{\uparrow} + F_{\downarrow}(W_{\uparrow} - V_{\uparrow}U_{\downarrow})]} (-IS_-) \\ &= (-IS_-) \frac{1}{1 - F_{\uparrow}U_{\uparrow} - F_{\downarrow}[V_{\downarrow} + F_{\uparrow}(W_{\downarrow} - V_{\downarrow}U_{\uparrow})]}, \end{aligned} \quad (\text{A11c})$$

$$\begin{aligned} t_{\downarrow\uparrow}^M &= \frac{1}{1 - F_{\uparrow}U_{\uparrow} - F_{\downarrow}[V_{\downarrow} + F_{\uparrow}(W_{\downarrow} - V_{\downarrow}U_{\uparrow})]} (-IS_+) \\ &= (-IS_+) \frac{1}{1 - F_{\downarrow}U_{\downarrow} - F_{\uparrow}[V_{\uparrow} + F_{\downarrow}(W_{\uparrow} - V_{\uparrow}U_{\downarrow})]}. \end{aligned} \quad (\text{A11d})$$

$V_{\uparrow}$  ( $V_{\downarrow}$ ) is the spin-diagonal component of the interaction between a carrier with  $\uparrow$  ( $\downarrow$ ) spin and the local potential on the  $M$  ion embedded in the medium of  $\Sigma_{\uparrow}$  ( $\Sigma_{\downarrow}$ ). A carrier with  $\uparrow$  ( $\downarrow$ ) spin which has already flipped in the previous scattering is subjected to  $U_{\uparrow}$  ( $U_{\downarrow}$ ) on the  $M$  ion embedded in the medium, wherein the  $d$  spin operator  $S_z$  is replaced by  $S_z - 1$  ( $S_z + 1$ ). Furthermore,  $W_{\uparrow}$  ( $W_{\downarrow}$ ) represents the interaction energy required by a carrier with  $\uparrow$  ( $\downarrow$ ) spin to flip and then reverse its spin.

## APPENDIX B: DYNAMICAL CPA — LOCATOR FORMALISM

### 1. CPA locator condition

In this subsection, we briefly outline an alternative but equivalent condition of the CPA, which is an extension

of the CPA using the locator formalism [33]. Assuming that the spin-dependent effective medium surrounds an arbitrary site  $n$ , we consider the transfer of the carrier with spin  $\mu$  between site  $n$  and the effective medium (i.e.,  $\Sigma_\uparrow$  and  $\Sigma_\downarrow$ ) by the site-renormalized interactor  $J_\mu$ . Then, the propagator  $G^A$  ( $G^M$ ) associated with the real potential of  $u_n^A$  ( $u_n^M$ ) embedded at site  $n$  in the medium is defined by

$$G^A = \frac{1}{\omega - u_n^A - \sum_\mu J_\mu a_{n\mu}^\dagger a_{n\mu}}, \quad (\text{B1})$$

$$G^M = \frac{1}{\omega - u_n^M - \sum_\mu J_\mu a_{n\mu}^\dagger a_{n\mu}}. \quad (\text{B2})$$

When we set the coherent potential  $\Sigma_\mu$  on the site  $n$  in the effective medium, the reference propagator,

$$P = \frac{1}{\omega - \sum_\mu \Sigma_\mu a_{n\mu}^\dagger a_{n\mu} - \sum_\mu J_\mu a_{n\mu}^\dagger a_{n\mu}}, \quad (\text{B3})$$

is equivalent to the Green function for the effective medium. Thus, the diagonal matrix element of  $P$  is equal

to  $F_\mu$  defined by Eq. (A2):

$$F_\mu(\omega) = \langle n\mu | P | n\mu \rangle = \frac{1}{\omega - \Sigma_\mu - J_\mu}. \quad (\text{B4})$$

Equation (B4) gives the relationship between  $J_\mu$  and  $F_\mu$ ;  $\mathcal{L}_\mu \equiv 1/(\omega - \Sigma_\mu)$  is called a locator. Hereafter, for the sake of simplicity, the site-diagonal elements in the Wannier representation  $\langle n\mu | G^A | n\nu \rangle$  are written as  $G_{\mu\nu}^A$  ( $\mu, \nu = \uparrow, \text{ or } \downarrow$ ). Then, the spin-diagonal element of  $G^A$  is given by

$$F_\mu^A(\omega) = G_{\mu\mu}^A = \frac{1}{\omega - E_A - J_\mu}, \quad (\text{B5})$$

and the spin-off-diagonal elements are  $G_{\uparrow\downarrow}^A = G_{\downarrow\uparrow}^A = 0$ . The site-diagonal elements of  $G^M$  are obtained after a somewhat complicated calculation using the commutation relationships between the components of  $\mathbf{S}$  but with no further approximations, as

$$G_{\uparrow\uparrow}^M = \frac{\omega - E_M - I(S_z + 1) - J_\downarrow}{[\omega - (E_M - IS_z) - J_\uparrow][\omega - E_M - I(S_z + 1) - J_\downarrow] - I^2[S(S+1) - S_z^2 - S_z]} \quad (\text{B6a})$$

$$G_{\downarrow\downarrow}^M = \frac{\omega - E_M + I(S_z - 1) - J_\uparrow}{[\omega - (E_M + IS_z) - J_\downarrow][\omega - E_M + I(S_z - 1) - J_\uparrow] - I^2[S(S+1) - S_z^2 + S_z]} \quad (\text{B6b})$$

$$G_{\uparrow\downarrow}^M = \frac{1}{[\omega - (E_M - IS_z) - J_\uparrow][\omega - E_M - I(S_z + 1) - J_\downarrow] - I^2[S(S+1) - S_z^2 - S_z]} (-IS_-) \quad (\text{B6c})$$

$$G_{\downarrow\uparrow}^M = \frac{1}{[\omega - (E_M + IS_z) - J_\downarrow][\omega - E_M + I(S_z - 1) - J_\uparrow] - I^2[S(S+1) - S_z^2 + S_z]} (-IS_+). \quad (\text{B6d})$$

Note that the site-diagonal elements of  $G^M$  involve spin operators. Thus,  $F_\mu^M(\omega)$  is defined as the thermal average of the spin-diagonal element  $G_{\mu\mu}^M$  by

$$F_\mu^M(\omega) = \langle G_{\mu\mu}^M \rangle = \sum_{S_z=-S}^S G_{\mu\mu}^M(S_z) \exp(\lambda S_z) / \sum_{S_z=-S}^S \exp(\lambda S_z), \quad (\text{B7})$$

where  $\lambda$  ( $\equiv h/k_B T$ ) is determined so as to reproduce a given value of  $\langle S_z \rangle$  [see Eq. (2.13)]. Note that the spin-off-diagonal elements  $\langle G_{\uparrow\downarrow}^M \rangle = \langle G_{\downarrow\uparrow}^M \rangle = 0$ , because  $G_{\uparrow\downarrow}^M$  ( $G_{\downarrow\uparrow}^M$ ) includes  $S_-$  ( $S_+$ ) in their final form. Finally, the CPA condition in the locator formula is given by

$$F_\mu(\omega) = (1-x)F_\mu^A(\omega) + xF_\mu^M(\omega). \quad (\text{B8})$$

When  $F_\mu$  is given,  $J_\mu$  is calculated by Eqs. (A2) and (B4) [i.e.,  $J_\mu = (\Delta^2/4)F_\mu$  for the model band defined by

Eq. (2.14)]. Then,  $F_\mu^A$  and  $F_\mu^M$  are calculated by Eqs. (B5) and (B7), and consequently,  $F_\mu$  is again obtained by Eq. (B8). Therefore,  $F_\mu$  and  $J_\mu$  are determined self-consistently.

## 2. Local DOS

The advantage of the locator formula CPA is that it is straightforward to determine species-resolved DOS, i.e., DOS associated with each kind of ion in the alloy. The local density of states (local DOS) at the  $A$  ( $M$ ) site is obtained by

$$D_\mu^A(\omega) = -\frac{1}{\pi} \text{Im} F_\mu^A(\omega), \quad (\text{B9a})$$

$$D_\mu^M(\omega) = -\frac{1}{\pi} \text{Im} F_\mu^M(\omega). \quad (\text{B9b})$$

In actual calculations, first we determined  $F_\mu$  and  $\Sigma_\mu$  by the  $t$  matrix formula CPA, and then calculated  $J_\mu$ , and consequently  $D_\mu^A(\omega)$  and  $D_\mu^M(\omega)$ . We numerically verified the relations

$$\int_{-\infty}^{\infty} D_\mu^A(\omega) d\omega = \int_{-\infty}^{\infty} D_\mu^M(\omega) d\omega = 1, \quad (\text{B10})$$

and

$$D_\mu(\omega) = (1-x)D_\mu^A(\omega) + xD_\mu^M(\omega), \quad (\text{B11})$$

which are a consequence of the CPA locator condition, Eq. (B8).

### 3. Spin-coupling strength $Q(\omega)$

We define the spin-coupling strength  $Q(\omega)$  as the normalized (negative) inner product between the carrier spin and localized spin on the  $M$  site: where  $D^M(\omega) = D_{\uparrow}^M(\omega) + D_{\downarrow}^M(\omega)$  and

$$\begin{aligned} C(\omega) &\equiv \sum_{\mu\nu} \langle \delta(\omega - H) a_{n\mu}^\dagger \sigma_{\mu\nu} \cdot \mathbf{S} a_{n\nu} \rangle \\ &= -\frac{1}{\pi} \left\langle \text{Im} \sum_{\mu\nu} \langle n\nu | G^M(\omega) | n\mu \rangle \langle n\mu | a_{n\mu}^\dagger \sigma_{\mu\nu} \cdot \mathbf{S} a_{n\nu} | n\nu \rangle \right\rangle \\ &= -\frac{1}{\pi} \text{Im} \langle (G_{\uparrow\uparrow}^M - G_{\downarrow\downarrow}^M) S_z + G_{\uparrow\downarrow}^M S_+ + G_{\downarrow\uparrow}^M S_- \rangle. \end{aligned} \quad (\text{B12})$$

- 
- [1] M. Takahashi, Phys. Rev. B **60**, 15858 (1999).  
[2] J. K. Furdya, J. Appl. Phys. **64**, R29 (1988).  
[3] K. C. Haas, *Semimagnetic Semiconductors and Diluted Magnetic Semiconductors*, edited by M. Averous and M. Balkanski (Plenum, New York) p. 59 (1991).  
[4] M. Takahashi, J. Phys.: Condens. Matter. **13**, 3433 (2001).  
[5] M. Takahashi, J. Phys. Soc. Jpn. **70**, 2224 (2001).  
[6] J. P. Lascaray, M. C. D. Deruelle, and D. Coquillat, Phys. Rev. B **35**, 675 (1987).  
[7] J. P. Lascaray, D. Coquillat, J. Deportes, and A. K. Bhattacharjee: Phys. Rev. B **38**, (1988) 7602.  
[8] A. K. Bhattacharjee, Solid State Comm. **65**, 275, (1988).  
[9] J. Szczytko, W. Mac, A. Stachow, A. Twardowski, P. Becla, and J. Tworzyclo, Solid State Comm. **99**, 927 (1996).  
[10] J. Okabayashi, A. Kimura, O. Rader, T. Mizokawa, A. Fujimori, T. Hayashi, and M. Tanaka, Phys. Rev. B **58**, R4211 (1998).  
[11] K. Ando, T. Hayashi, M. Tanaka, and A. Twardowski, J. Appl. Phys. **53**, 6548 (1998).  
[12] J. Szczytko, W. Mac, A. Twardowski, F. Matsukura, and H. Ohno, Phys. Rev. B **59**, 12935 (1999).  
[13] H. Ohno: J. Magn. Magn. Mater. **200**, 110 (1999).  
[14] M. Takahashi and K. Kubo, Phys. Rev. B **66**, 153202 (2002).  
[15] M. Takahashi and K. Mitsui, Phys. Rev. B **54**, 11298 (1996).  
[16] A. Gonis, *Green Functions for Ordered and Disordered Systems* (North-Holland, Amsterdam) Studies in Mathematical Physics, Vol. 4<sup>th</sup>, (1992).  
[17] H. Ehrenreich and L. M. Schwartz, *Solid State Physics, Advances in Reseach and Application* ed. H. Ehrenreich, F. Seitz and D. Turnbull (New York, Academic) **31** p. 149. (1976).  
[18] Y. Onodera, and Y. Toyozawa, J. Phys. Soc. Jpn. **24**, 341 (1968).  
[19] M. Cardona and D. L. Greenway, Phys. Rev., **133A**, 1685 (1964).  
[20] M. C. Cohen and T. K. Bergstresser, Phys. Rev., **141**, 489 (1966).  
[21] S. Sanvito, P. Ordejón, and N. A. Hill, Phys. Rev. B, **63**, 165206 (2001).  
[22] S. I. Gubarev and M. G. Tyazhlov, Sov. Phys. Solid States, **36**, 373 (1990).  
[23] M. Zielinski, C. Rigaux, A. Mycielski, and M. Menant, Phys. Rev. B, **63**, 035202 (2000).  
[24] J. P. Lascaray, *Semimagnetic Semiconductors and Diluted Magnetic Semiconductors* edited by M. Averous and M. Balkanski (Plenum, New York), p. 169 (1991).  
[25] A. Twardowski, M. Nawrocki, and J. Ginter, Phys. Stat. Sol. (b), **96**, 497 (1979).  
[26] M. Shirai, T. Ogawa, I. Kitagawa, and N. Suzuki, J. Magn. Magn. Mater. **177-181**, 1383 (1998).  
[27] J. H. Park, S. K. Kwon, and B. I. Min, Physica B **281 & 282**, 703 (2001).  
[28] M. Linnarsson, E. Janzen, B. Monemar, M. Kleverman, and A. Thilderkvist: Phys. Rev. B **55**, 6938 (1997).  
[29] J. Okabayashi, A. Kimura, O. Rader, T. Mizokawa, A. Fujimori, T. Hayashi, and M. Tanaka, Phys. Rev. B **64**, 125304 (2001).  
[30] J. Okabayashi, A. Kimura, O. Rader, T. Mizokawa, A. Fujimori, T. Hayashi, and M. Tanaka: Physica E **10**, 192 (2001).  
[31] A. Oiwa, S. Katsumoto, A. Endo, M. Hirakawa, M. Iye, H. Ohno, F. Matsukura, A. Shen, and Y. Sugawara,

- Solid State Comm. **103**, 209 (1997).
- [32] A. Oiwa, S. Katsumoto, A. Endo, M. Hirakawa, M. Iye, F. Matsukura, A. Shen, Y. Sugawara, and H. Ohno, Physica B **249-251**, 775 (1998).
- [33] K. Kubo: J. Phys. Soc. Jpn. **36**, 32 (1974).